Proceedings of the ASME 2011 Dynamic Systems and Control Conference
DSCC2011
October 31 - November 2, 2011, Arlington, VA, USA

DSCC2011-6194

STOCHASTIC MODELLING OF DROP COALESCENCE ON NON-POROUS SUBSTRATES FOR INKJET APPLICATIONS

J. William Boley*
School of Mechanical Engineering
Purdue University
West Lafayette, Indiana 47907
Email: jwboley@purdue.edu

Robert A. Sayer
School of Mechanical Engineering
Purdue University
West Lafayette, Indiana 47907

George T.-C. Chiu
School of Mechanical Engineering
Purdue University
West Lafayette, Indiana 47907

ABSTRACT

Coalescence between two drops on a substrate is one of the important factors that can affect print quality in inkjet applications. Two stochastic models (constant contant angle mode and constant contact area mode) that consider drop placement error, drop impact, and drop evaporation are proposed for determining the probability of coalescence between adjacently printed drops on nonporous substrates. Experiments are conducted to measure the probability of coalescence with respect to deposition time difference between adjacently printed drops and compared to the predictions of the models. The measured coalescence follows the constant contact angle mode evaporation model during the initial phase of the life of the first drop, which is followed by a mix between the constant contact angle mode and the constant contact area mode models for the remainder of the life of the first drop. This study shows that for probabilities of coalescence between 10% *and* 80% *the constant contact angle mode model can be used to determine deposition time difference threshold values for adjacent drops in applications promoting drop coalescence while the constant contact area mode model can be used for applications avoiding drop coalescence. Further efforts are needed to capture the dynamics of the mixed-model evaporation and to more accurately predict larger (greater than* 80%*) and smaller (less than* 10%*) occurrences of coalescence.*

INTRODUCTION

If two liquid drops are put into contact at low relative velocities so inertial effects can be neglected relative to surface tension effects, then the interface separating the two bodies bursts resulting in excess surface-energy, which causes an unstable situation driving the system towards a new equilibrium shape [1]. This physical phenomenon is known as coalescence.

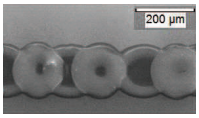

Figure 1. SEM IMAGE OF PD ALKANETHIOLATE LINE PRINTED WITH TWO PASSES OF THE PRINT-HEAD.

Coalescence between two drops on a substrate is one of the key physical phenomena that can affect print quality in inkjet applications. The literature shows two separate approaches when addressing the coalescence of adjacent drops on a substrate. The first is to avoid coalescence by allowing time for ink solvent to evaporate before depositing ink onto an adjacent pixel. Figure 1 is a scanning electron microscope (SEM) image of a printed line of Pd alkanethiolate printed with 2 passes for printed electronic applications. This approach resulted in resistance measurements comparable to photolithographic fabrication of the same material [2]. The bottom layer of spots were printed on the first pass. After waiting some time, the spaces between the drops printed on the first pass are filled by the print-head on the second pass, thus resulting in the completed image. It can be seen that the adjacent dots overlap but have not merged; the dots have separate boundaries. This method is used to preserve dot placement and dot gain by limiting the interaction between adjacently printed drops [3–5]. Although this approach has been shown to work, no specific guidlines have been provided on how long to wait between deposition of adjacent drops so that overlap occurs but coalescence does not.

Stringer and Derby [6] produced stable lines with parallel

*Address all correspondence to this author.

sides by depositing individual drops on a surface so that they coalesce. They found the stable line (bead) width to fall between an upper and lower bound. The minimum stable bead width was determined by the maximum drop spacing for stable coalescence while maximum stable bead width was determined by the minimum drop spacing below which a bulging instability occurred. In addition to comparison to existing experimental results, the approach was tested using a silver nanoparticle ink as well as an organometallic ink. The experimental results matched the theory for all inks except for the organometallic ink. The authors attributed this discrepancy to the high evaporation rate of the organic solvent due to its high vapor pressure. Although an order of magnitude calculation was provided for evaporation of the organic solvent, Stringer and Derby [6] did not address the details of the evaporation dynamics. In addition, drop placement and drop volume variation were not considered. Soltman et. al. [7] demonstrated a methodology to optimize the inkjet printing of two-dimensional, partially wetting films. In this study they propose a scheme that adjusts line-to-line spacing to guarantee coalescence between lines occurs so that a two dimensional bead's contact angle is between its advancing and retreating values as it is printed. The proposed scheme includes a derived equation for the bead's surface with pinned contact lines and a semi-empirical fit for mass loss due to evaporation. To fit the evaporation data, a constant contact area mode evaporation equation proposed by Hu and Larson was used [8]. The model is the result of running finite element simulations for a range of contact angles and fitting the results to a polynomial function of contact angle. It was shown to fit experimental data and the theoretical model proposed by Picknett and Bexon to within about 1%. Alternatively, the Picknett and Bexon model can be used to account for mass losses due to evaporation. As was the case with the work by Stringer and Derby, the uncertainties associated with the volume and placement of the droplets were not considered. Additionally, constant contact angle mode evaporation was not addressed, which may be the case for a variety of printed materials.

Typical variations in drop placement and drop volume. The size of inkjet droplets is often in the size range where Brownian motion can significantly alter the certainty of drop placement (e.g. a mean deviation of $3.1\mu m$ for $5.0\mu m$ diameter drops falling for $1s$ in air) [9], causing the position of an inkjet deposited drop to become a random variable. Slight random variations in fluid flow through the nozzle and within the ink reservoir during the drop formation process results in random drop volumes. The dynamics associated with determining the occurrence of coalescence between two adjacently printed drops depends on the drops' placements and volumes [10]. This causes the coalescence of adjacently printed drops to be a stochastic process with respect to the difference in their deposition times.

In a previous publication [10] a stochastic coalescence model assuming constant contact angle mode evaporation was proposed, which determined the probability of coalescence between two adjacent drops as a function of the difference in their deposition times by considering random drop placement error, drop impact, and sessile drop evaporation. Subsequently [11] used this model to invoke timing constraints to avoid drop coalescence between adjacently printed drops. However, the model [10] did not consider constant contact area mode sessile drop evaporation and drop volume variation, which is not the case in general.

This paper extends the work of [10] by discussing the model assumptions and their validity, by considering constant contact area mode as well as constant contact angle mode sessile drop evaporation and by considering variations in drop volume. In addition, we describe experiments conducted in order to characterize initial contact angle prior to evaporation and to measure the probability of coalescence to compare to the prediction of the models.

The remainder of the paper is organized as follows. Assumptions for the model and experimental validation are listed and discussed. Next, the details of the problem are given in the problem formulation section. Then the dynamics of a drop drying on a substrate are given. In addition, simulations of the proposed models are provided. The models described herein are then validated experimentally. Lastly, concluding remarks are made.

ASSUMPTIONS

For this coalescence model, we assume the following:

1. The deposited drops have a circular footprint.
2. Drops impact the substrate in the deposition regime (i.e. the drop deforms and stays attached to the substrate without any break up) [12].
3. Drop mass losses on the substrate are governed by diffusive evaporation under standard temperature and pressure.
4. The substrate uniformity and the drop impact dynamics are such that the contact angle for the drop just prior to evaporation is not a random variable, resulting in the variation of the initial radius of the drop on the substrate to be caused soley by variation in the drop volume.
5. Drop mass losses during flight and impact are negligible.

The first assumption is inherent in the models chosen which describe a drop impacting a substrate [13] and a sessile drop drying on a substrate [14]. These models assume that the drops make a circular footprint on the substrate. In general, this may not be the case. In fact, other studies have been conducted showing the drop footprint can stray from that of a circle depending on the print-head scan speed [15] and the drop drying dynamics [16]. Bernal et. al. showed that increasing the print-head scan speed increases dot elongation, tails, and satellites. However, their study suggests a circular footprint is a reasonable assumption at print-head scan speeds less than $762mm/s$ ($30in/s$).

The second assumption is also for applicability of the drop impact and drop evaporation models. This is a natural assumption since inkjet printing applications require the stability associated with deposition type drop impact. In general, there are

at least five other classifications of drop impact (prompt splash, corona splash, receding breakup, partial rebound, and rebound) [12]. However, the ink and substrate properties are typically tuned so that deposition type impact is guaranteed, thus validating this assumption.

Assumption three implies that mass losses due to convection are negligible and that there is no external heating source, which is valid for all printing applications except for a small set of applications that control coffee ring formation by varying the substrate temperature [7].

No literature has been found to directly support assumption four. However, it will be shown in the experimental section that this assumption leads to a variation in volume that is expected with inkjet deposition.

The fifth assumption is used in the experimental validation section. To investigate the validity of this assumption, the evaporation of a drop in a fluid stream is considered [17]. The drop is approximated as a sphere during the time of flight. This is a good approximation since the amount that the drops deform from perfect spheres is negligible for drop diameters less than $100\mu m$ [9], which is larger than the drop diameters for inkjet applications. The methods of mass transfer from the drop to the surrounding fluid are diffusive mass transfer and convective mass transfer. Mass transfer due to radiative heating of the drop is neglected since there is typically no source of radiation in the inkjet process. The Appendix shows the details of the development of the equations and analyses used to validate this assumption. The results showed that mass loss as a percentage of initial drop mass increases with increased drop flight distance, increased solvent vapor pressure, decreased ejection velocity, and decreased initial drop volume. Using a conservative value for the ejection velocity ($1m/s$) for $27pL$ drops of toluene (drop volume and solvent used in our experiments) with a flight distance of $1mm$ (approximate distance traveled in our experiments) results in less than 2% drop volume lost during flight, which is less than the drop volume variation obtained from the experimental section of this paper.

PROBLEM FORMULATION

Figure 2 is a top view schematic of two adjacent drops deposited onto a substrate by an inkjet printer. These drops could be produced by the same nozzle or by two separate nozzles. The subscripts of the coordinates and radii give the order in which the drops were deposited (i.e. subscript 1 denotes the first drop deposited while subscript 2 denotes the second drop deposited). Each drop has a nominal centroid $(\overline{X}_i, \overline{Y}_i)$, a positional uncertainty $(\Delta X_i, \Delta Y_i)$, a nominal radius $\overline{R}_i$, and an uncertainty in the radius ΔR_i. In our previous work [10] the following condition is used to ensure coalescence will not occur.

$$\begin{cases} \sqrt{(X_1-X_2)^2+(Y_1-Y_2)^2} \\ -(R_1(t)+\max_t R_2(t)) > 0, & \text{if } R_1(t) > 0 \\ R_1(t) = 0, & \text{otherwise} \end{cases} \quad (1)$$

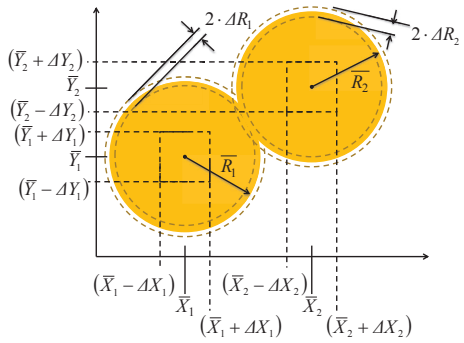

Figure 2. TOP VIEW OF TWO ADJACENT DROPS ON A SUBSTRATE

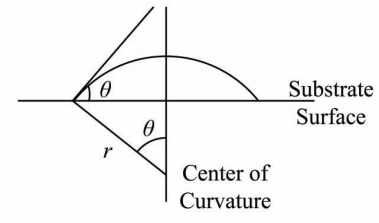

Figure 3. SIDE VEW OF SESSILE DROP ON A SUBSTRATE

This is a conservative approach because the first drop will be evaporating during the spreading process of the second drop. However, this approximation is valid since the collision dynamics are faster than the evaporation dynamics [14, 18]. This study considers the drop placement and the drop impact in the same manner as our previous work [10]. However, to account for a wider range of applications, we now consider constant area mode sessile drop evaporation in addition to constant contact angle mode sessile drop evaporation.

DROP DRYING ON A SUBSTRATE

In order to capture the dynamics of the radius of the first drop due to evaporation, the sessile diffusion model proposed by Picknett and Bexon [14] will be used. Figure 3 shows a sessile drop on a substrate with a radius of curvature, r and contact angle θ. Let $m_d(t)$ be the mass of the liquid drop, θ_0 be the contact angle of stabilized drop on the substrate prior to evaporation, $R_1(0)$ be the initial sessile drop radius, and $m_d(0)$ be the initial sessile drop mass. Then the radius of the wet area of the first drop as a function of time can be found as [14]

$$R_1(t) = \left(\frac{3m_d(t)}{\pi\rho_d(1-\cos\theta)^2(2+\cos\theta)}\right)^{\frac{1}{3}} \sin\theta = r\sin\theta; \quad (2)$$

where

$$\frac{dm_d(t)}{dt} = -\frac{qE(C/r)m_d^{\frac{1}{3}}(t)}{2\rho_d^{\frac{1}{3}}} \tag{3}$$

for constant contact angle mode evaporation and

$$\frac{dm_d(t)}{dt} = -\frac{qE(C/r)m_d^{\frac{1}{3}}(0)\sin\theta_0}{2\rho_d^{\frac{1}{3}}\sin\theta} \tag{4}$$

for constant contact area mode evaporation, where $E^3 = 3/(\pi(1-\cos\theta_0)^2(2+\cos\theta_0))$ and $q = 4\pi D(c_0 - c_i)$. The ratio C/r can be empirically determined as $C/r = 0.6366\theta_0 + 0.09501\theta_0^2 - 0.06144\theta_0^3$, for $0 \leq \theta_0 \leq 0.175$ radians or for $0.175 \leq \theta_0 \leq \pi$ radians, $C/r = 0.00008957 + 0.6333\theta_0 + 0.1160\theta_0^2 - 0.08878\theta_0^3 + 0.01033\theta_0^3$; where C is the capacitance of an equiconvex lens whose centerline is the substrate/surface interface shown in Fig. 3.

For constant contact angle mode evaporation, Eq. (2) simplifies to

$$R_1(t) = E\left(\frac{m_d(t)}{\rho_d}\right)^{\frac{1}{3}}\sin\theta_0. \tag{5}$$

Integrating Eq. (3) and plugging into Eq. (5) gives

$$R_1(t) = \frac{E\sin\theta_0}{\rho_d^{\frac{1}{3}}}\sqrt{m_d^{\frac{2}{3}}(0) - \frac{qE(C/r)}{3\rho_d^{\frac{1}{3}}}t}. \tag{6}$$

For constant contact area mode evaporation, the radius, $R_1(t)$ is constant until all of the drop has evaporated, in which case it is zero. The only parameter changing due to evaporation is θ. Todorov [19] showed that the governing equation to describe the change in θ with respect to time during constant contact area evaporation is

$$\frac{d\theta}{dt} = -\frac{4q}{\pi\rho_d}\frac{1}{R_1^2(0)}\frac{\cos^3(\theta/2)}{\sin(\theta/2)}\frac{C}{r}; \tag{7}$$

where $R_1^2(0)$ can be found using Eq. (2). Integrating Eq. (7) gives

$$t = -\frac{\pi\rho_d}{4q}R_1^2(0)\int_{\theta_0}^{\theta_1}\frac{\sin(\theta/2)}{\cos^3(\theta/2)(C/r)}\,d\theta; \tag{8}$$

where θ_1 is contact angle at time t during this mode of evaporation. For example, if t is the time for the drop to evaporate entirely, then $\theta_1 = 0$. Todorov went on to approximate Eq. (8) by using a 6 term power series expansion of the integrand, resulting in

$$t = -\frac{\pi\rho_d R_1^2(0)}{2q}\left\{\begin{array}{l} 6.9233(\theta/2)^2 + 2.0541(\theta/2)^3 \\ -16.2512\ln(2.0463 - \theta/2) \\ +\ln(1.2658 + \theta/2) \end{array}\right\}_{\theta=\theta_0}^{\theta=\theta_1} \tag{9}$$

if $0 \leq \theta \leq 0.175$ radians and

$$t = -\frac{\pi\rho_d R_1^2(0)}{2q}\left\{\begin{array}{l} 29.4661(\theta/2) + 3.4285(\theta/2)^2 \\ +62.6456\tan^{-1} \\ (0.50593(-5.2661 + \theta) \\ +1.4097\ln(0.9688 + \theta/2)) \\ +57.014\ln(-7.9096 \\ +5.2661(\theta/2) - (\theta/2)^2) \end{array}\right\}_{\theta=\theta_0}^{\theta=\theta_1} \tag{10}$$

if $0.175 \leq \theta \leq \pi$ radians. For implementation, the $\{\}_{\theta=\theta_0}^{\theta=\theta_1}$ denotes that the expression should be calculated first for $\theta = \theta_0$, then for $\theta = \theta_1$ and their difference should be taken. It follows that the dynamics of the radius $R_1(t)$ for constant contact area mode evaporation are as follows

$$R_1(t) = \begin{cases} R_1(0) & \text{for } t < t_f \\ 0 & \text{for } t \geq t_f \end{cases} \tag{11}$$

where t_f is the time required for the drop to fully evaporate ($\theta_1 = 0$) and can be computed by Eqs. (9) and (10).

MODEL SIMULATION

For each time (t) after stabilization of the first drop, given the distribution of ΔX_i, ΔY_i, and the variation in the initial drop volume, Monte Carlo simulation can be performed to compute the probability of the occurrence of coalescence using Eq. (1), where $\max_t R_2$ is obtained from the methods described in previous work [10] and $R_1(t)$ from Eq. (6) for constant contact angle mode evaporation and Eq. (11) for constant contact area evaporation. This resulting probability gives a constraint on the firing time between nozzles on the printhead.

Although Monte Carlo simulation is used in this study given the experimentally obtained drop placement error distribution, more analytical approaches can be employed if theoretical distributions of the random variables are available.

Printing water on glass in dry air will be used to demonstrate the utility of the proposed model. All parameters used for this simulation can be found in a previous work [10] with the exception of the drop volume variation ($\pm 5\%$). This example reflects the inkjet system in the Purdue lab. When dealing with drops printed on a substrate, coalescence can occur between

drops printed adjacently in the vertical direction, the horizontal direction, or along the diagonal. For this simulation, coalescence is considered between two drops, each from a separate nozzle. For this example simulation one drop comes from the third nozzle (x and y standard deviations are $11.4\mu m$ and $12.5\mu m$, respectively) and the other comes from the sixth nozzle (x and y standard deviations are $13.3\mu m$ and $20\mu m$, respectively) from a 12-nozzle print-head. To cover all possible inkjet related arrangements, relative drop positions simulated were alignment in the media advance direction, the print-head scan direction, and diagonally. Simulations were run for both modes of evaporation. Figure 4 shows the Monte Carlo simulation results using the model. Forty equally spaced time samples from 0 to 1 second. For each time sample, $100,000$ uniformly selected random samples were taken from the distributions for X_1, X_2, Y_1, Y_2, and the initial volume. The x axis of Fig. 4 represents the time elapsed between when the first drop stabilizes and the when the second drop is deposited. The y axis is the probability that the two drops will coalesce. As projected, the probability decreases as time increases. The simulations show that constant contact area mode evaporation (Const. Area, shown with dashes) is more conservative than the constant contact angle (Const. Angle, shown without dashes) for all cases, which is expected since the drop's radius will not decrease until the drop has evaporated entirely. The probability curves follow the same trend for alignment in the media advance direction (Horiz.) and the print-head scan direction (Vert.) but not for diagonal alignment (Diag.). In fact, the diagonally aligned drops have a much lower probability of coalescence because the nominal center-to-center distance between diagonally aligned drops is a factor of $\sqrt{2}$ larger than that of those aligned in the media advance or print-head scan directions. Other variations in probability of coalescence depend solely on the error distribution for each of the nozzles.

Using this model, given an acceptable coalescence probability the minimum or maximum printing time between adjacent drops can be determined. Given the minimum or maximum print time, the print-head scan speed, distance between nozzle columns in a nozzle array, and the nozzle resolution, one can then compute the minimum distance between pixels in a print mask that can be printed on the same pass, as shown in [11].

EXPERIMENTAL VALIDATION AND DISCUSSION

Experiments were conducted to characterize the drop volume distribution, obtain the initial contact angle prior to evaporation and to measure the probability of coalescence to compare to the predictions of the models. All print experiments were conducted using the printing system described in [2, 20, 21].

Contemporary methods for drop volume characterization involves the use of a high speed, high magnification camera [22]. Another approach has been used here. A large number, of drops of a solution of known concentration are jetted at a stable frequency onto a piece of foil of known mass. The mass of the foil is then measured after all of the solvent has evaporated. The

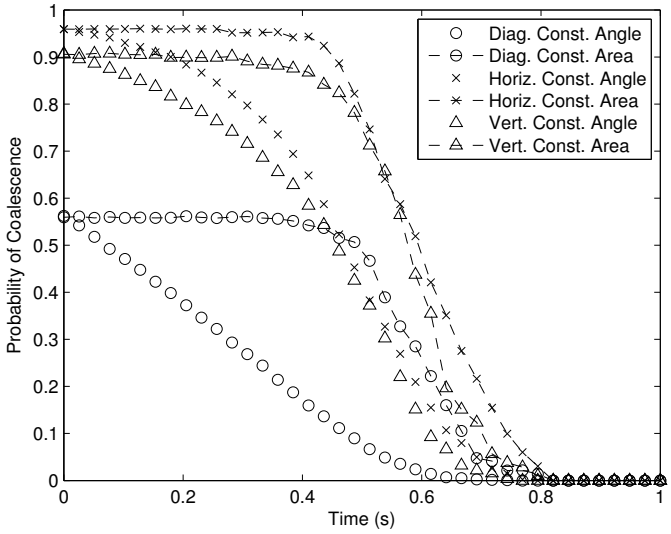

Figure 4. COALESCENCE MODEL SIMULATION FOR WATER ON GLASS

mass difference before and after jetting gives the mass of the solute deposited onto the foil. Using the known concentration and number of drops, the mean drop volume can be computed by

$$\text{drop volume} = \frac{\text{mass difference}}{\text{concentration} \times \text{number of drops}}. \qquad (12)$$

For example, 12×10^4 drops of Pd hexadecanethiolate at approximately $50mM$ ($37.08g/L$) were jetted at $500Hz$ onto a piece of foil with an initial mass of $27.884mg$ (all mass measurements were made using an Orion®Cahn®C-33 microbalance). The mass of the foil after the solvent evaporated was measured to be $28.003mg$. This resulted in a mean drop volume of $27pL$.

In order to characterize the contact angle and the volume distribution, a spot radius distribution was obtained from a grid of drops printed as shown in Fig. 5. Using assumptions 3 and 5 and Eq. (2), the contact angle prior to evaporation can be found by numerically solving

$$\cos^3\theta_0 - 3\cos\theta_0 + \left(2 - \frac{3\overline{V}(0)}{\pi \overline{R_1}^3(0)}\right) = 0; \qquad (13)$$

where $V(0) = \frac{m_d(0)}{\rho_d}$ is the volume of the drop prior to evaporation, $\overline{V}(0)$ is the mean drop volume prior to evaporation found by Eq. (13), and $\overline{R_1}(0)$ is the mean sessile drop radius prior to evaporation found by taking the mean of the radius of the solute spots (Fig. 5) left behind on the substrate after solvent evaporation.

The resulting initial contact angles for 50mM Pd hexadecanethiolate on Al layered Si, Kapton®300 FPC, and Si were

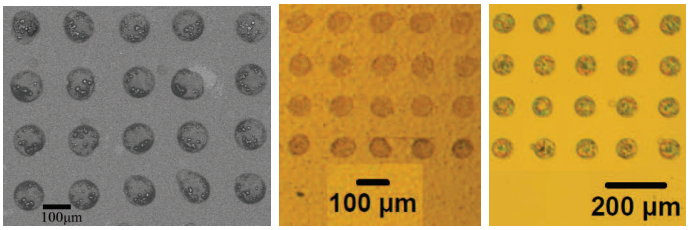

(a) AL LAYERED SI (b) KAPTON®300 FPC (c) SI

Figure 5. PRINTED ARRAYS FOR INITIAL SESSILE DROP RADIUS CHARACTERIZATION

10.1°, 42.3°, and 43.1°, respectively. Note that the method for obtaining the drop radius distribution is based on the assumption that the footprint of the solute is the same as the footprint of the sessile drop just after drop stabilization and prior to drop evaporation. Given the contact angle found in Eq. (13) and the distribution of $R_1(0)$ and using Eq. (2), the distribution of $V(0)$ can be found by

$$V(0)_i = \frac{\pi}{3}\overline{R_1}^3(0)(1-\cos\theta_0)^2(2+\cos\theta_0); \qquad (14)$$

where i goes from 1 up to the total number of drops in the grid printed for obtaining the sessile drop radius distribution prior to evaporation. The mean of the voume distributions obtained from Eq. (14) differed from the measured mean volume obtained from Eq. (12) by less then 1% in all cases. In addition, all cases exhibited a resulting drop volume distributionthe 95% uncertainty was less than 13%, which is consistent with the drop volume variation found in thermal inkjet print-heads.

A separate experiment was conducted in order to measure the probability of coalescence versus deposition time difference between two adjacently printed drops. Figure 6 shows a representative image of the print experiment used. An array of pairs of drops was printed for a fixed print-head scan speed at a fixed spacing. Next, the array was examined for coalescence under an SEM. It was observed that there were three types of outcomes to this experiment:

1. Full coalescence - when the two drops merge into one drop
2. Partial coalescence - when a liquid bridge has noticeably formed between the two drops
3. No coalescence - when there are two distinct drops with no liquid bridge.

Figure 7 shows these three outcomes for 50mM Pd hexadecanethiolate on Al layered Si. The main indication of no drop coalescence is the distinct boundary between overlapping drops implying that no liquid bridge has formed. If a printed pair of drops falls under the full coalescence outcome or the partial coalescence outcome, then the two drops are said to have coalesced; otherwise they are said to have not coalesced.

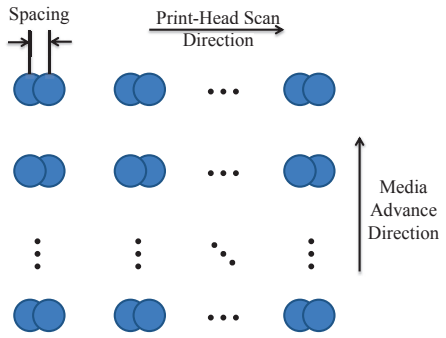

Figure 6. SCHEMATIC OF PRINT PATTERN FOR MEASURING COALESCENCE

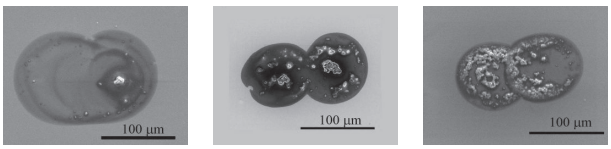

(a) FULL COALESCENCE (b) PARTIAL COALESCENCE (c) NO COALESCENCE

Figure 7. SEM IMAGES OF COALESCED DROP EXAMPLES

The total number of coalescence events is found for each printed array and then divided by the total number of printed pairs. This result is the measured probability of coalescence. The experiment is then repeated for different print-head scan speeds (i.e. different deposition time differences), to obtain a measured probability of coalesce versus time. This experiment was conducted for Pd hexadecanethiolate on Al layered Si with a spacing of $60\mu m$ for print-head scan velocities resulting in deposition time differences of $0.05, 0.1, 0.15, \ldots, 0.4s$. The uncertainty in the velocities was $\pm 0.005mm/s$. All drops were printed from the second nozzle (x and y standard deviations of $11.3\mu m$ and $11.6\mu m$, respectively) of a 12-nozzle print-head. For comparison, the predicted probabilities for constant contact angle and constant contact area are also included. Figure 8 shows the measured results for the coalescence experiments. The error bars for the experimental result are at 95% confidence.

As shown in Fig. 8, the measured coalescence follows the same trend as the constant contact angle model during the early stages of evaporation of the first drop (at $0.05s$ and $0.1s$). The measured coalescence then diverges from the constant coalescence model. This is as expected because the contact line of the first drop for some classes of solvents which are initially unpinned at low concentrations, resulting in constant contact angle mode evaporation until enough solvent has evaporated causing the local viscosity at the contact line to increase to the point where the contact line will stick [23]. Following this, the contact line in general can do one or any combination of the following throughout the rest of the evaporation process [23]:1) Remain pinned (constant contact area evaporation), 2)remain pinned until the local viscosity diverges causing the contact line to separate

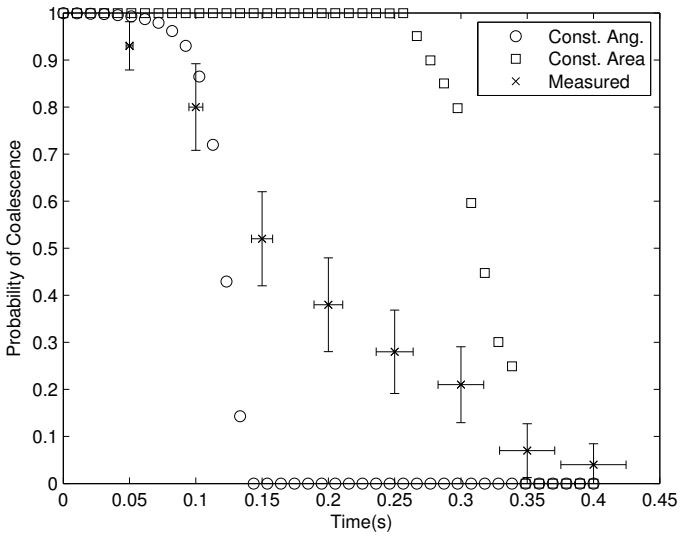

Figure 8. MODEL VALIDATION: PD HEXADECANETHIOLATE ON AL LAYERED SI

from the solute deposits, resulting in a return to constant contact angle evaporation, and 3) Slowly reced while the contact angle decreases (neither the area or the contact angle are constant). This series of evaporation mode transitions is known a mixed evaporation mode [14]. The measured results show that the first drop evaporates under mixed mode evaporation from $0.1s$ until the remainder of the first drop's life. However, the exact dynamics of the contact line are unknown. In general, the contact line dynamics will depend upon many parameters (e.g.'s solvent vapor pressure, initial solute concentration, ink visosity, substrate roughness, etc.). Therefore, additional efforts are needed to better understand the motion of the contact line. The result in Fig. 8 shows that the combination of the two models forms a boundary after $0.1s$ prior to $0.35s$. Inside this interval ($0.1s$ to $0.35s$) the constant contact angle model can be used to conservatively estimate the maximum deposition time difference for applications requiring a minimum occurrence of coalescence while the constant contact area model can be used to conservatively estimate the minimum deposition time difference for applications prescribing a maximum occurrence of coalescence. However, more work is needed to improve the applicability of the models for coalescence probabilities above 80% and below 10%.

CONCLUSIONS

A stochastic model for drop coalescence on non-porous substrates was proposed. Simplifying assumptions were made and discussed. Simulations were run considering constant contact angle and constant contact area evaporation with different drop alignments. Experiments were conducted to characterize the drop volume distribution, obtain the initial contact angle prior to evaporation and to measure the probability of coalescence to compare to the predictions of the models. From the experiment, it is evident that the constant contact angle model is applicable for applications promoting coalecsence and the constant contact area model is applicable for avoiding coalescence. However, more work is needed in order to capture the mixed mode dynamics of the contact line and to improve the applicability of the models for coalescence probabilities above 80% and below 10%.

ACKNOWLEDGMENT

The authors would like to thank Hewlett-Packard for providing the thermal inkjet nozzles and Stephen L. Hodson for making the Pd Hexadecanethiolate for the experiments conducted in this work.

REFERENCES

[1] Menchaca-Rocha, A., Martinez-Davalos, A., Nunez, R., Popinet, S., and Zaleski, S., 2001. "Coalescence of liquid drops by surface tension". *Physical Review E,* **63**(4, Part 2), APR, pp. art. no.–046309.

[2] Bhuvana, T., Boley, W., Radha, B., Dolash, B. D., Chiu, G., Bergstrom, D., Reifenberger, R., Fisher, T. S., and Kulkarni, G. U., 2010. "Inkjet printing of palladium alkanethiolates for facile fabrication of metal interconnects and surface-enhanced Raman scattering substrates". *Micro & Nano Letters,* **5**(5), OCT, pp. 296–299.

[3] Yen, J., Carlsson, M., Chang, M., Garcia, J., and Nguyen, H., 2000. "Constraint solving for inkjet print mask design". *Journal of Imaging Science and Technology,* **44**(5), SEP-OCT, pp. 391–397.

[4] Yen, J., Lin, Q., and Wong, P., 1999. Print masks for inkjet printers. US Patent 5,992,962.

[5] Boley, W., Bhuvana, T., Hines, B., Sayer, R. A., Chiu, G., Fisher, T. S., Bergstrom, D., Reifenberger, R., and Kulkarni, G. U., 2009. "Inkjet Printing Involving Palladium Alkanethiolates and Carbon Nanotubes Functionalized with Single-Strand DNA". pp. 824–827. 25th International Conference on Digital Printing Technologies, Louisville, KY, SEP 20-24.

[6] Stringer, J., and Derby, B., 2010. "Formation and Stability of Lines Produced by Inkjet Printing". *Langmuir,* **26**(12), JUN 15, pp. 10365–10372.

[7] Soltman, D., Smith, B., Kang, H., Morris, S. J. S., and Subramanian, V., 2010. "Methodology for Inkjet Printing of Partially Wetting Films". *Langmuir,* **26**(19), OCT 5, pp. 15686–15693.

[8] Hu, H., and Larson, R., 2002. "Evaporation of a sessile droplet on a substrate". *Journal of Physical Chemistry B,* **106**(6), FEB 14, pp. 1334–1344.

[9] Lee, E. R., 2003. *Microdrop Generation*. CRC Press, Washington, D.C.

[10] Boley, J. W., Ariyur, K., and Chiu, G. T.-C., 2010. "Coalescence Constraints for Inkjet Print Mask Optimization".

pp. 1 – 6. IEEE/ASME International Conference on Advanced Intelligent Mechatronics, AIM, Montreal, QC, Canada, JUL 6-9.

[11] Boley, J., and Chiu, G., 2009. "Print Mask Design for Maximum Throughput Subject to Print Quality Constraints". 25th International Conference on Digital Printing Technologies, Austin, TX, SEP 19-23.

[12] Rioboo, R., Tropea, C., and Marengo, M., 2001. "Outcomes from a drop impact on solid surfaces". *Atomization and Sprays,* **11**(2), MAR-APR, pp. 155–165.

[13] PasandidehFard, M., Qiao, Y., Chandra, S., and Mostaghimi, J., 1996. "Capillary effects during droplet impact on a solid surface". *Physics of Fluids,* **8**(3), MAR, pp. 650–659.

[14] Picknett, R. G., and Bexon, R., 1977. "Evaporation of Sessile or Pendant Drops in Still Air". *Journal of Colloid and Interface Science,* **61**(2), pp. 336–350.

[15] Bernal, E., Allebach, J. P., and Pizlo, Z., 2007. "Improved pen alignment for bidirectional printing". *Journal of Imaging Science and Technology,* **51**(1), pp. 1–22.

[16] Bhardwaj, R., Fang, X., and Attinger, D., 2009. "Pattern formation during the evaporation of a colloidal nanoliter drop: a numerical and experimental study". *New Journal of Physics,* **11**, JUL 31.

[17] Ranz, W. E., and Marshall, W. R., 1952. "Evaporation from Drops. 1.". *Chemical Engineering Progress,* **48**(3), pp. 141–146.

[18] Lim, T., Han, S., Chung, J., Chung, J. T., Ko, S., and Grigoropoulos, C. P., 2009. "Experimental study on spreading and evaporation of inkjet printed pico-liter droplet on a heated substrate". *International Journal of Heat and Mass Transfer,* **52**(1-2), JAN 15, pp. 431–441.

[19] Todorov, S., 2002. "On the dynamics of sessile drop evaporation". *Dokladi na B'garskata Akademiya na Naukite,* **55**(1), pp. 41–44.

[20] Post, N. J., 2007. "Precision Micro-Deposition of Functional Layers Using Inkjet Drop-On-Demand and Applications to the Functionalization of Microcantilever Sensors". MS Thesis, Purdue University, West Lafayette, IN, AUG.

[21] Kumar, V., Boley, J. W., Ekowaluyo, H., Miller, J. K., Marvin, G. C., Chiu, G. T.-C., and Rhoads, J. F., 2010. "Linear and nonlinear mass sensing using piezoelectrically-actuated microcantilevers". Vol. 1, pp. 571 – 579. Society for Experimental Mechanics - SEM Annual Conference and Exposition on Experimental and Applied Mechanics, Indianapolis, IN, JUN 7-9.

[22] Chen, A., and Basaran, O., 2002. "A new method for significantly reducing drop radius without reducing nozzle radius in drop-on-demand drop production". *Physics of Fluids,* **14**(1), JAN, pp. L1–L4.

[23] Frastia, L., Archer, A. J., and Thiele, U., 2011. "Dynamical Model for the Formation of Patterned Deposits at Receding Contact Lines". *PHYSICAL REVIEW LETTERS,* **106**(7).

APPENDIX

An approximation for the rate of mass lost from the drop during flight due to convection and diffusion can be found by the average Sherwood number, defined as

$$\overline{Sh} = \frac{\overline{K}d}{D}; \tag{15}$$

where d is the drop diameter (characteristic length for a sphere), D is the diffusive mass transfer coefficient and $\overline{K}$ is the average mass transfer coefficient, which can be expressed as

$$\overline{K} = \frac{\frac{dm_d}{dt}}{A(c_0 - c_i)}; \tag{16}$$

where A is the effective mass transfer area and m_d is the mass of the drop. Using Eqs. 15, 16 and the Froessling equation for a sphere [17] yields

$$\frac{dm_d}{dt} = -\alpha_1 m_d^{1/3} - \alpha_2 m_d^{1/2} U^{1/2}; \tag{17}$$

where $\alpha_1 = 2.0D\pi^{2/3}(c_0 - c_i)\left(\frac{6}{\rho_d}\right)^{1/3}$,
$\alpha_2 = 0.6\left(\frac{\rho_f}{\mu_f}\right)^{1/6}\left(\frac{6}{\rho_d}\right)^{1/2} D^{2/3}\pi^{1/2}(c_0 - c_i)$, ρ_d is the density of the drop, ρ_f is the density of the fluid medium, U is the relative velocity of the drop in the fluid stream, and μ_f is the dynamic viscosity of the fluid medium.. Typical inkjet drop ejection speeds are much higher than the drop's terminal velocity, causing U to be time dependent. The dyanamics of U can be captured by using the relaxation time constant, τ [9], which is

$$\tau = \frac{d^2\rho_d}{18\mu_f}. \tag{18}$$

Assuming drop ejection occurs parallel to gravity, we have

$$U = \tau g + (U_0 - \tau g)e^{-\frac{t}{\tau}}; \tag{19}$$

where U_0 is the drop ejection speed and g is the gravitational acceleration. Combining Eqs. (18) and (19) and plugging into Eq. (17) yields

$$\begin{aligned}\frac{dm_d}{dt} = &-\alpha_1 m_d^{1/3} \\ &-\alpha_2 m_d^{1/2}\left\{\begin{array}{l}\alpha_3 m_d^{2/3} \\ +(U_0 - \alpha_3 m_d^{2/3})e^{-\alpha_4 t m_d^{-2/3}}\end{array}\right\}^{1/2};\end{aligned} \tag{20}$$

where $\alpha_3 = \left(\frac{6}{\pi}\right)\left(\frac{\rho_d^{1/3}}{18\mu_f}\right)g$ and $\alpha_4 = \left(\frac{\pi}{6}\right)^{2/3}\left(\frac{18\mu_f}{\rho_d^{1/3}}\right)$.